

Electronic Supplementary Information (ESI)

Controlled Synthesis of MFe₂O₄ (M = Mn, Fe, Co, Ni and Zn) Nanoparticles and Their Magnetic Properties.

Jeotikanta Mohapatra,¹ A. Mitra,² D. Bahadur,^{1, 3,*} M. Aslam^{1, 2,*}

¹ Centre for Research in Nanotechnology and Science (CRNTS)

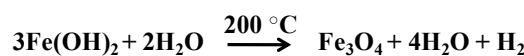
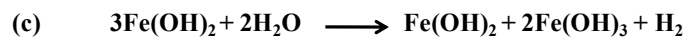
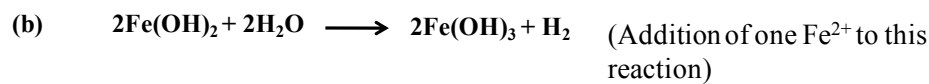
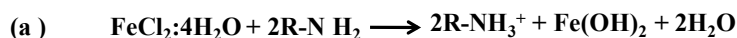
² Department of Physics,

³ Department of Metallurgical Engineering and Materials Science,
Indian Institute of Technology Bombay, Powai, Mumbai-400076, India

*To whom correspondence should be addressed. E-mail: m.aslam@iitb.ac.in. Phone: +91 22 2576 7585, dhirenb@iitb.ac.in.

A. Synthesis of spinel-oxide Nanoparticles:

The magnetite nanoparticles were produced from Fe²⁺ ion in the presence of excess oleylamine. It is well-known that Fe²⁺ ion can be oxidized easily using H₂O.^{1a} Ferrous chloride that have been used for the reaction is hydrated (FeCl₂:4H₂O). We believe that this water moiety assists the formation of Fe(OH)₂. This Fe(OH)₂ hydrated ions (Fe²⁺) get converted to Fe(OH)₃ through the Schikorr's reaction,¹ which ultimately leads to formation of stable magnetite (Fe₃O₄) phase.



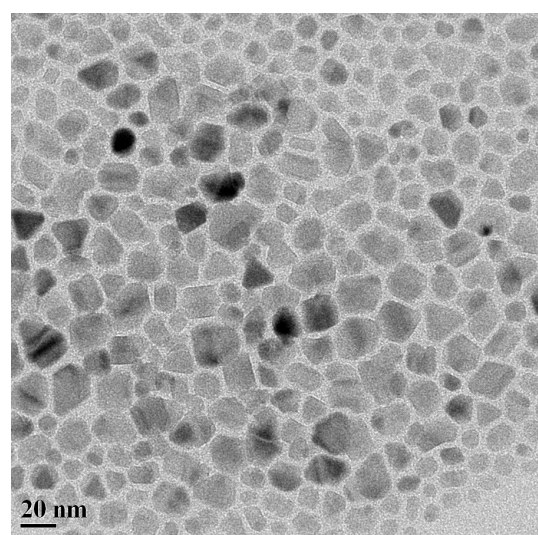


Fig. S1: TEM images of MnFe₂O₄ nanoparticles produced with precursor to amine mole ratio 1:2. It confirms particle size above 9 nm (with monodispersion) cannot be produced through changing the molar ratio of precursor to amine.

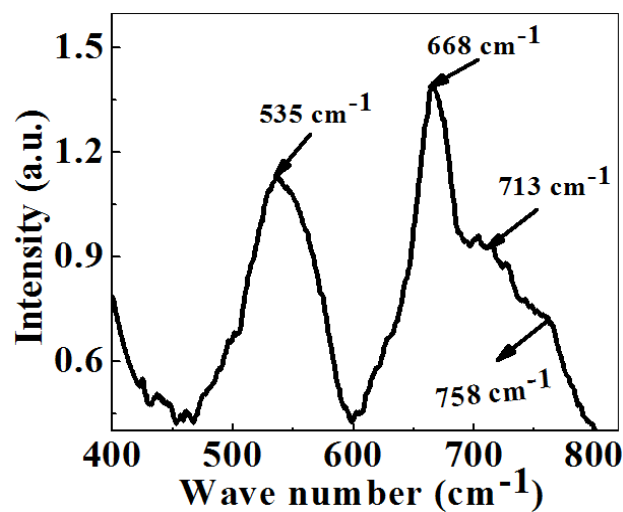


Fig. S2 Raman spectra of the synthesized magnetite nanoparticles. The most prominent band centered at 668 cm^{-1} (A_{1g}) corresponds to the symmetric stretching of oxygen atoms along the Fe-O bonds. The prominent shoulder peaks at 713 cm^{-1} and 758 cm^{-1} are generally attributed to the surface oxide layer formation due to the laser beam heating or aging. The peak observed at 535 cm^{-1} is assigned to T_{2g} vibration of magnetite.²

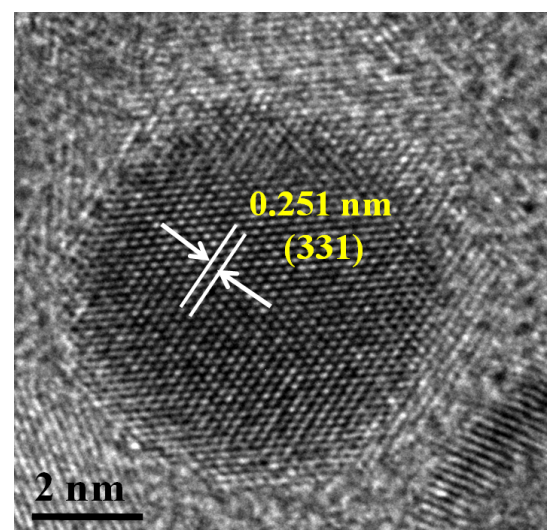


Fig. S3 HRTEM images of 6 nm Fe_3O_4 nanoparticles showing their high crystalline nature.

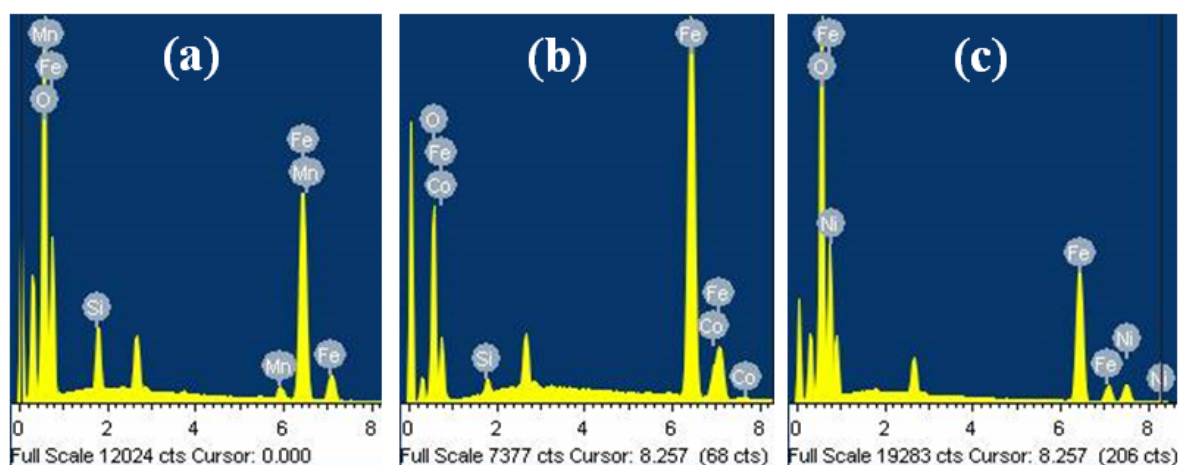


Fig. S4 Energy dispersion spectrum (EDS) of (a) MnFe_2O_4 , (b) CoFe_2O_4 and (c) NiFe_2O_4 nanoparticles.

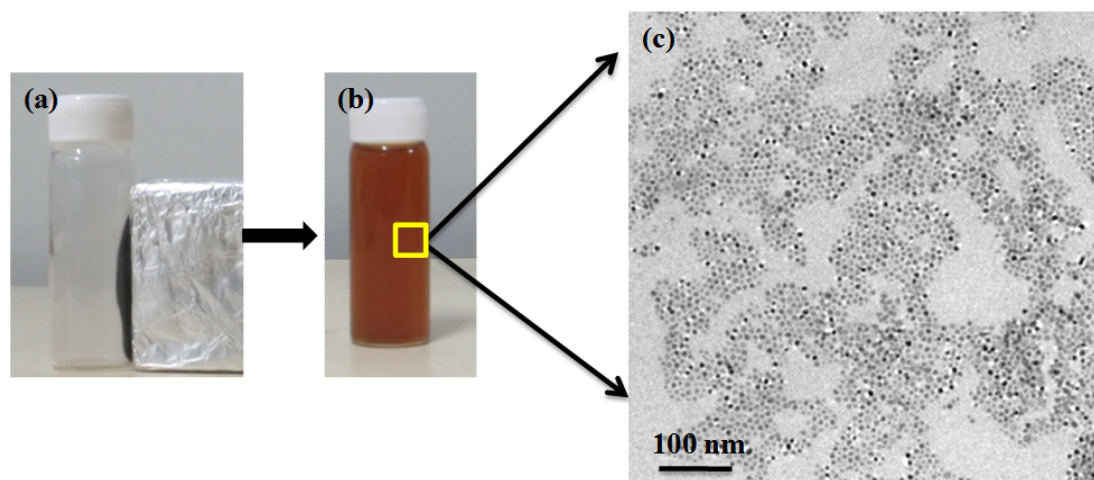


Fig. S5 (a) A photograph showing magnetic capture of MnFe_2O_4 nanoparticles, (b) nanoparticles dispersed in Hexane for TEM imaging and (c) Large area TEM micrograph shows the particles size distribution

B. Variation of Blocking Temperature with nanoparticles size

For non-interacting single domain MNPs the magnetic relaxation time is given by³

$$t = \tau_0 \exp [KV / k_B T] \dots\dots\dots(1)$$

where K is the anisotropy constant, V is volume of nanoparticles and τ_0 is a characteristic constant of particles related to gyromagnetic precession.

When the relaxation time 't' compared to the timescale of the experimental technique one measures an average value of the magnetization, but if the relaxation time is long compared to the timescale of the experimental technique, one measures the instantaneous value of the magnetization. The superparamagnetic blocking temperature is defined as the temperature at which the superparamagnetic relaxation time equals the timescale of the experimental technique and is given by

$$T_B = \frac{KV}{k_B \ln(t_m / \tau_0)} \dots\dots\dots(2)$$

From the above equation it is clear that the magnetocrystalline anisotropy (K) and the volume (V) of magnetic nanoparticles are the two key parameters on which blocking temperature depends. Larger the nanoparticles size, larger is ' $k_B T$ ' required for superparamagnetic transition. Therefore, T_B increases with increasing nanoparticle size and the experimental data also shows the same trend.

C. Size dependent magnetization properties

The relationship between the saturation magnetization (M_s), nanoparticle diameter (d) and the thickness of inactive layer (t) is

$$M_S = M_{S(bulk)} \left(1 - 6 \frac{t}{d} \right) \dots \dots \dots (3)$$

Here, t is the thickness of the shell and M_s is equal to 89 emu/g. The results of our magnetization studies show a linear decrease in inactive layer thickness with respect to particle size as shown in Fig. S4.

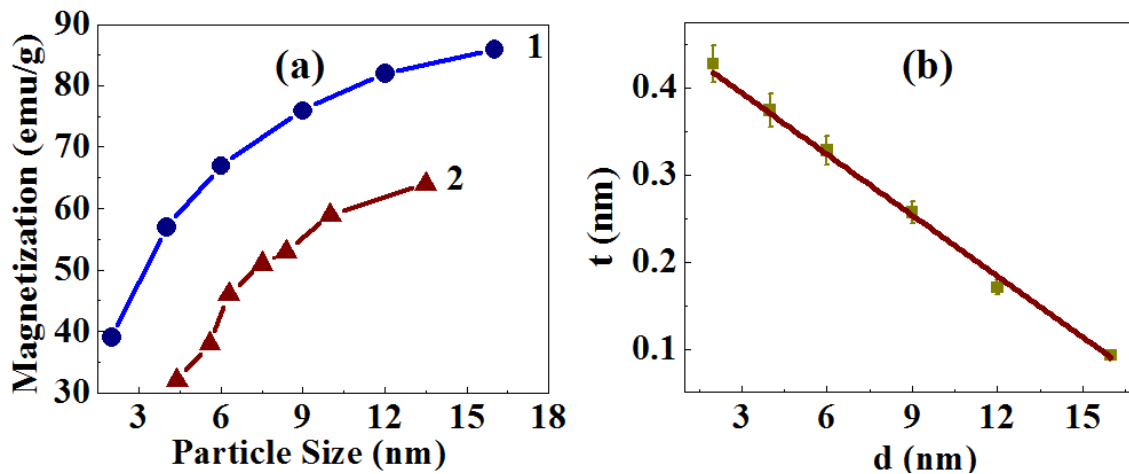


Fig. S6 (a) Comparison of the reported magnetization values and experimental data of MnFe_2O_4 nanoparticle: line 1 represents experimental data and line 2 represents the earlier reported data.⁴

(b) Inactive layer thickness of MFe_2O_4 nanoparticles decreases with the increase of nanoparticle size.

D. FTIR spectroscopy analysis

The freshly prepared OAm, OA and TOPO functionalized nanoparticles are characterized via FTIR spectroscopy (Fig.S5 A and B). The IR spectra of OAm functionalized nanoparticles exhibit the characteristic NH₂ scissoring and N–H stretching bands of oleylamine groups at 1605 cm⁻¹ and 3140 cm⁻¹ respectively.⁵ After the surface modification of nanoparticles with OA and TOPO we can see the absence of the NH₂ scissoring and N–H stretching bands, which indicates the successful replacement of amine moiety by OA and TOPO. In OA-functionalized nanoparticles, multiple bands at 1455, 1105 and 1024 cm⁻¹ are observed corresponding to the different vibrational modes of C–O=C bonds.⁶ Whereas, in TOPO functionalized nanoparticles the strong band at 1020 cm⁻¹ is assigned to –P–O stretching mode of phosphine oxide.⁷ This confirms the successful exchange of surface ligand.

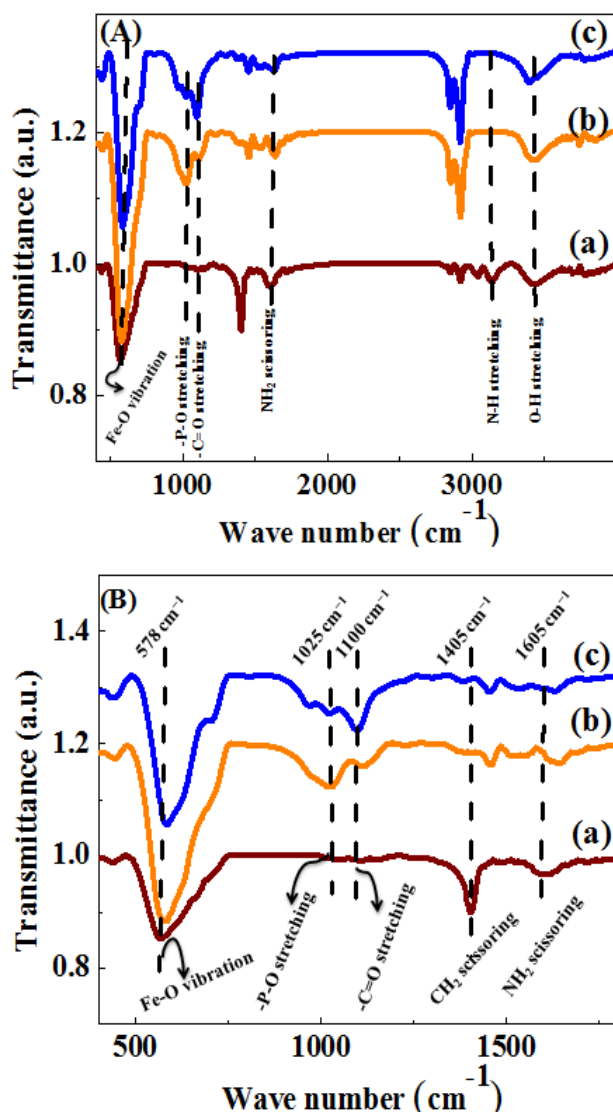


Fig. S7 (A) a, b and c represents the FTIR spectra of OAm, OA and TOPO functionalized 6 nm MnFe₂O₄ nanoparticles, respectively. (B) Is the low frequency region of OAm, OA and TOPO functionalized MnFe₂O₄ nanoparticles.

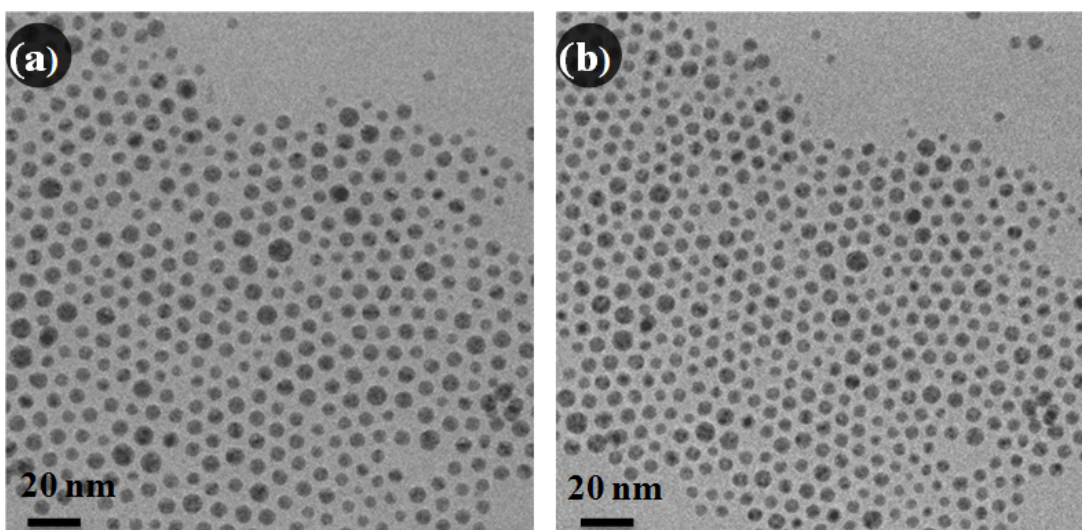


Fig. S8: TEM images of MnFe_2O_4 nanoparticles: (a) before ligand exchange (amine functionalized nanoparticles); (b) after ligand exchange with oleic acid.

E. Correction of magnetic measurements by TGA analysis

In TGA analysis of OAm, OA and TOPO functionalized MnFe_2O_4 nanoparticles (Fig. S9) we found around 9.5 %, 10 % and 17 % weight loss due to: (i) the removal of physically adsorbed water molecules and trace solvent molecules (below 215 °C) and (ii) decomposition of organic molecules (in the range 215–400 °C).^{8,9} All the magnetic measurements are plotted after subtracting this weight fraction of non-magnetic organic layer from the sample weight utilized for the magnetic measurements.

The number of surfactant molecules on each particle can be roughly estimated by the formulation¹⁰

$$N = \frac{wN_A\rho \frac{4}{3}\pi R^3}{(1-w)M}$$

Where N is the number of surfactant molecules attached on nanoparticle surface, R is the mean radius of magnetite nanoparticles, ρ is the density of magnetite material, N_A is Avogadro's

number, M is the molecular weight of surfactant and ‘w’ is the weight loss. An average estimation reveals approximately 125, 130 and 132 number of OAm, OA and TOPO molecules are passivating each 6 ± 0.5 nm particles.

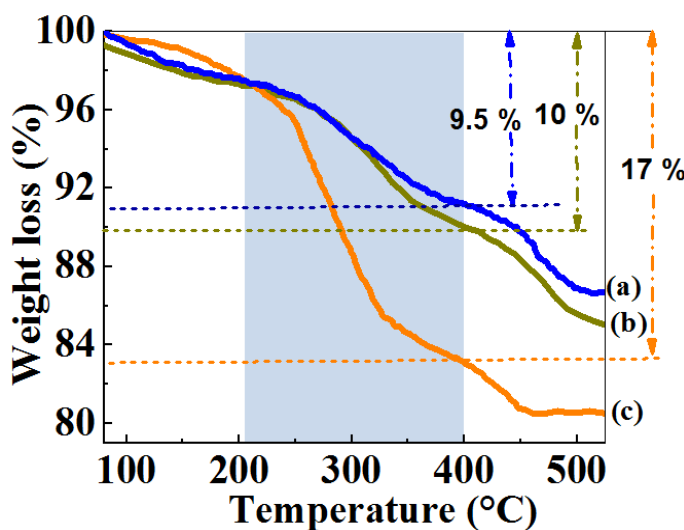


Fig. S9: (a), (b) and (c) represents the TGA plot of OAm, OA and TOPO functionalized 6 nm MnFe₂O₄ nanoparticles, respectively. The highlighted region represents the percentile weight loss due to the decomposition of respective surfactant molecules.

Table 1 Lattice parameters of MFe₂O₄ (M = Mn, Fe, Co, Ni, Zn) nanoparticles prepared with amine to metal chloride mole ratio 5:1.

Sample Code	Peak Position (311) (Degree)	Estimated d ₃₁₁ from XRD (nm)	Estimated d ₃₁₁ from SEAD pattern (nm)
ZnFe ₂ O ₄	35.60	0.2505	0.2502
NiFe ₂ O ₄	35.62	0.2529	0.2500
CoFe ₂ O ₄	35.48	0.2528	0.2513
MnFe ₂ O ₄	35.44	0.2531	0.2540
Fe ₃ O ₄	35.49	0.2530	0.2536

References

1. (a) G. Schikorr, Z. Allg. Chem., 212 (1938), p. 33. (b) A. Košak, D. Makovec, M. Drofenik and A. Žnidaršič, *J. Magn. Magn. Mater.* 2004, **272-276**, 1542. (c) R. M. Cornell, U. Schwertmann, The Iron Oxides: Structure, Properties, Reactions, Occurrences and Uses, 2nd edition, p.536.
2. (a) D. Bersani, P. P. Lottici and A. Montenero, *J. Raman Spectrosc.*, 1999, **30**, 355. (b) I. Chamritski and G. Burns, *J. Phys. Chem. B*, 2005, **109**, 4965.
3. Q. Song and Z. J. Zhang, *J. Am. Chem. Soc.* 2004, **126**, 6164.
4. C. Liu and Z. J. Zhang, *Chem. Mater.* 2001, **13**, 2092.
5. Z. Xu, C. Shen, Y. Hou, H. Gao and S. Sun, *Chem. Mater.*, 2009, **21**, 1778.
6. M. Lattuada and T. A. Hatton, *Langmuir*, 2007, **23**, 2158.
7. T. J. Daou, J. M. Grenèche, G. Pourroy, S. Buathong, A. Derory, C. Ulhaq-Bouillet, B. Donnio, D. Guillon and S. Begin-Colin, *Chem. Mater.*, 2008, **20**, 5869.
8. C. E. Astete, C. S. S. R. Kumar, C. M. Sabliov, *Colloids Surf. A*, 2007, **299**, 209.
9. Y. Hou, J. Yu and S. Gao, *J. Mater. Chem.*, 2003, **13**, 1983.
10. S. Verma and D. Pravarthana, *Langmuir*, 2011, **27**, 13189.